J. Fluid Mech. (1974), *vol.* 62, *part* 1, *pp.* 65–84
Printed in Great Britain

Turbulent shear flow in a curved duct

By L. B. ELLIS AND P. N. JOUBERT
Department of Mechanical Engineering, University of Melbourne

(Received 13 April 1971 and in revised form 4 May 1973)

Experiments were conducted in two curved rectangular ducts of different radii and the results compared with flow in a straight duct. The turbulent boundary layers developing on the curved walls were examined for mean flow properties. The law of the wall takes a modified form and the usual logarithmic portion applies over a very small range of the profiles on the inner walls and a slightly larger range on the outer walls. Similarity based on a defect law did not exist for any part of the flow examined.

1. Introduction

The order-of-magnitude arguments usually applied to boundary layers indicate that curvature, and hence the resultant transverse pressure gradient, is of secondary importance and can therefore be neglected for 'mild' curvature. Schultz-Grunow & Breuer (1965), Yen & Toba (1961) and Murphy (1962) have pointed out that this reduces the boundary-layer approximation to a lower order in the case of curved flow. Some work has been done in obtaining solutions to the higher-order equations (with the curvature terms included) for the laminar boundary-layer case. Schultz-Grunow & Breuer give a comparative summary of some of the methods employed.

In the turbulent boundary-layer case further factors are present. Eskinazi & Yeh (1956), Traugott (1958) and others showed that flow curvature has a marked effect on the turbulence of a shear flow, a not unexpected result in view of the classical observations of Taylor (1922, 1932) and Görtler (1941), and more recently Thomann (1968) and Tillman (1967), on the differences in the stability of curved shear flows.

Wattendorf (1935) and Eskinazi & Yeh have shown that, even with relatively mild curvature, there is considerable deviation from the logarithmic 'law of the wall' as compared with the equivalent case in plane flow. Wattendorf attempted to correlate his observed shear stress distribution with those obtained from eddy viscosity concepts and also on the basis of an assumed angular momentum mixing length. Neither of these approaches agreed with his results.

Marris (1956, 1960) postulated that Taylor's vorticity transfer theory had greater validity for curved duct flows. He developed relationships that contained a number of free parameters, thus allowing considerable latitude in matching empirical data, but the values so obtained seem to lack universality.

Rotta (1967), in a theoretical investigation of the effect of streamwise wall curvature on compressible boundary layers, assumed values for the charac-

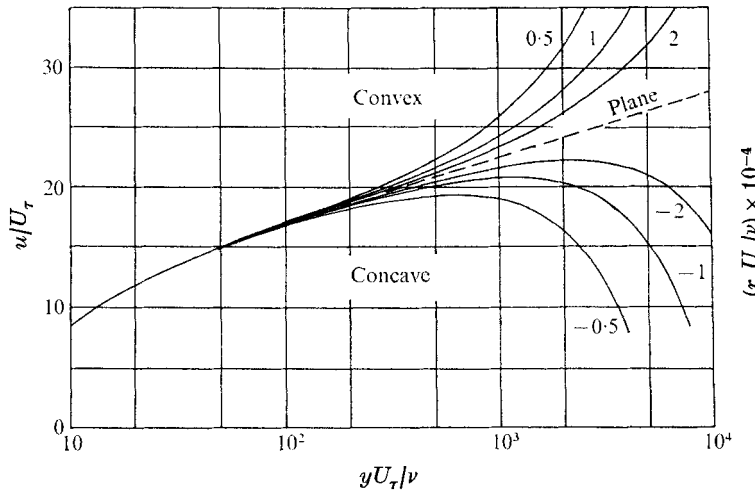

FIGURE 1. Velocity distributions of incompressible turbulent flow near curved walls (from Rotta 1967).

teristic length of the eddy structure, enabling the momentum and energy equations to be solved numerically. The results for the simpler incompressible case are reconstructed here as figure 1 (generally the same as Rotta 1967, figure 3). These curves are quantitatively in agreement with Eskinazi & Yeh's results, although Rotta noted that his treatment underestimated the effect of curvature. In the experiments of Wattendorf and Eskinazi & Yeh, the ducts used were of relatively short radius and, in the case of the latter, the reported tests were limited to one Reynolds number. Both the experiments were arranged with the curved duct following a straight channel with fully developed flow.

The purpose of the work discussed here was to investigate (i) differences between flow developing in straight and curved ducts starting from an undeveloped flow; (ii) the effect of mild curvature on highly developed channel flow, particularly with regard to the existence of flow similarity; (iii) the effect of wall curvature on a boundary layer with zero streamwise pressure gradient.

2. Analysis

The use of u/U_τ and yU_τ/ν as wall region co-ordinates is known to produce similarity that is universal for plane, smooth-wall boundary layers, with and without longitudinal pressure gradients, and which, with an appropriate slip function, correlates rough-wall boundary layers as well.

For the smooth wall

$$u/U_\tau = f(yU_\tau/\nu). \tag{1}$$

Various hypotheses and dimensional reasoning (Rotta 1962) result in a logarithmic law applicable in a region just outside the viscous sublayer:

$$\frac{u}{U_\tau} = \frac{1}{\mathscr{K}} \ln \frac{yU_\tau}{\nu} + A. \tag{2}$$

Multiplying by U_τ/U_1, where U_1 is a reference velocity, typically the maximum or free-stream velocity, yields

$$\frac{u}{U_1} = \frac{1}{\mathscr{H}}\frac{U_\tau}{U_1}\ln\frac{yU_1}{\nu} + \frac{1}{\mathscr{H}}\frac{U_\tau}{U_1}\ln\frac{U_\tau}{U_1} + \frac{U_\tau}{U_1}A, \tag{3}$$

which is the basis of the Clauser chart (Clauser 1954). In the case of curved flow, it is possible that (2) is invalid owing to the presence of an additional variable, but the experimental results of Eskinazi &Yeh indicate that it is valid for at least a small region just outside the viscous sublayer.

In considering the core region of fully developed channel flow, the implication of the findings of Traugott, that solid body rotation produces effects on the turbulence quantities, is that similarity based on angular velocity defect is unlikely to occur. Likewise, a similarity argument based on a velocity defect can be dismissed, on the grounds that the experimental evidence of Wattendorf and others indicates that there is a considerable region of near potential-like velocity distribution. In such a region, the velocity distribution would be a function of the datum velocity. On the other hand, this criticism does not apply to similarity based on the ur distribution. Using $K = ur$ the defect law relationship would be

$$K = K_0 + k_0\phi(\xi), \tag{4}$$

where K_0 is the correlating ur product and ξ the position co-ordinate, say

$$(r-r_1)/(r_2-r_1).$$

Townsend (1956) noted, when discussing flow similarity with concentric rotating cylinders, that a large body of the core region is close to being irrotational; while close to the wall, the mean rate of shear is so large that any superimposed rotation is negligible.

Kinney (1967) accepted Taylor's vorticity transport theory as being relevant to rotating flows. His approach, when applied to the core region of curved duct flows by the authors, yielded

$$\frac{u_m/r_m - u/r}{U_\tau/r_m} = \pm\frac{((r_m/r_1)^2-1)^{-\frac{1}{2}}}{2K_4}\left(\ln\left(\frac{r_m}{r}+\left(\left(\frac{r_m}{r}\right)^2-1\right)^{\frac{1}{2}}\right)-\frac{r_m}{r}\left(\left(\frac{r_m}{r}\right)^2-1\right)^{\frac{1}{2}}\right), \tag{5}$$

where K_4 is a universal constant, and r_m is the radius to the point of zero shear stress. r_m can be eliminated by using the wall shear stress at both walls, since

$$r_m^2 = (\tau_{\omega 2}-\tau_{\omega 1})\Big/\left(\frac{\tau_{\omega 2}}{r_1^2}-\frac{\tau_{\omega 1}}{r_2^2}\right). \tag{6}$$

Equation (5) is a defect law based on angular velocity and, as such, is at variance with the experimental observations of Traugott and the discussion that led up to (4).

3. Experimental programme

The layout of the equipment used was generally as shown in figure 2, the outer wall of the 15 in. radius duct being made adjustable so as to allow the imposition of a zero or variable pressure gradient on the inner-wall boundary layer.

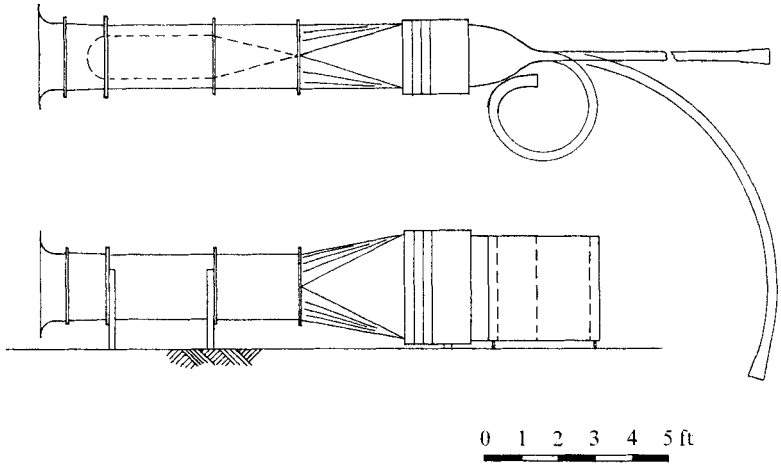

FIGURE 2. Experimental apparatus.

The duct height of 33 in. and width of 2·5 in. were selected as a compromise based on the air flow available, the desirability of a large width to allow a reasonable thickness of boundary layer, and the desirability of a narrow width, to minimize secondary flow effects, ensure full development of the flow in the length available, to avoid separation at entry or exit and to prevent the effect of entry and exit conditions extending for any appreciable length into the duct.

All ducts were fitted with wall static tappings at positions corresponding to 30° intervals on the 15 in. radius duct. For the curved ducts, tappings were placed in both the inner and outer walls. In addition to the main tappings, which were arranged along the equatorial section, one row was also provided along a line at right angles to these, to assist in checking the two-dimensionality of the flow. The bulk of the velocity readings were taken with a 0.014 in. thick, flattened, square-ended total head probe and a 0·030 in. dia. static head probe, although some early readings in the straight duct made use of a 0·024 in. dia. square-ended total head tube. The total and static tubes were calibrated against a standard Pitot-static tube. These tubes were mounted on a rigid, micrometer-type traverse. The effective total head tube position was obtained by adding a correction to the physical position, the correction being that established by MacMillan (1957).

The wall shear stresses were determined by using a Clauser chart. This method, like those using Preston or Stanton tubes, relies on the existence of a universal wall region. Townsend reported that the wall stresses deduced on the basis of the logarithmic wall law are consistent with the stresses measured in other ways; and the work of Eskinazi & Yeh indicates that this contention is valid at least for the degree of wall curvature considered here.

During preliminary checking with the 15 in. radius duct fitted, it was found that there were gross irregularities, similar to those found by Marris, in the velocity profiles. Furthermore, there was considerable inconsistency between profiles taken at various off-centre positions across the duct. Careful checking of misalignments in the duct geometry and rearrangement of the screens with a lower

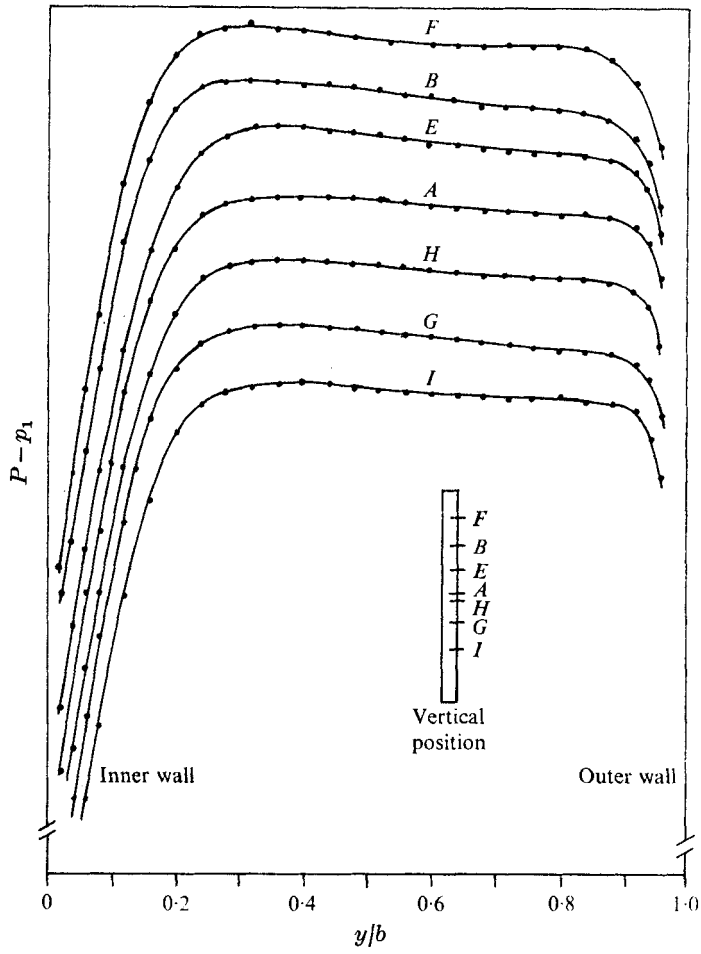

FIGURE 3. Profiles at various spanwise positions, 210° station (after modification).

solidarity, as suggested by Bradshaw (1965), removed these irregularities (see Ellis 1969). Figure 3 shows the profiles at various spanwise positions at the 210° station after these corrections. The results of the traverses for the stations from 30° to 210° indicated that the flow may not have been fully developed at the 210° station, and this would not be reasonably guaranteed even when a station was provided at 230°.

Trials were then made of methods of promoting rapid thickening of the boundary layer in the entrance length of the duct. 6 in. wide strips of $\frac{1}{2}$–60 emery paper proved successful, to the extent that the velocity profiles at the 210° and 230° stations were essentially identical and showed no spanwise variation. While the emery paper would undoubtedly have altered the turbulence structure downstream, it is likely such alteration would have decayed in the distance to the measuring station.

In the case of the 75 in. radius duct spanwise variation in velocity was noted and this persisted despite careful realigning of the duct and, in fact, was stable

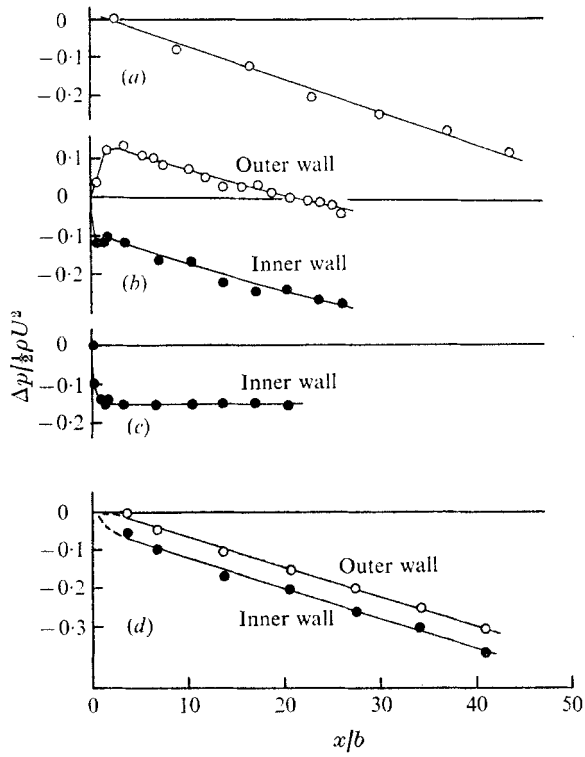

FIGURE 4. Wall static pressure against position along duct. Duct (in. radius): (*a*) straight; (*b*) 15; (*c*) 15 (set for zero pressure gradient); (*d*) 75.

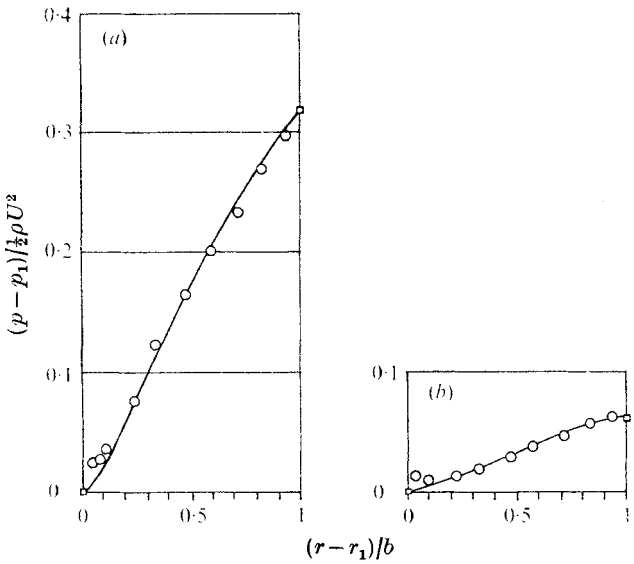

FIGURE 5. Typical radial static pressure distributions. Duct (in. radius): (*a*) 15; (*b*) 75. ——, calculated values. ○, static probe readings; □, wall static pressure.

against quite gross duct distortions and deliberate attempts to induce asymmetric flow. Although the profiles for the stations immediately on each side of the equatorial station were identical within the limits of the accuracy of the measurements, those further out showed considerable variation. After all known methods that might correct the spanwise variation had been tried, they were accepted as part of the flow. Kaye & Elgar (1958) and Tani (1962) reported Taylor–Görtler type vortices in curved turbulent flow; and it is felt that disturbances of this type may have contributed to these irregularities.

4. Results and discussion

Figure 4 shows the dimensionless plots of wall static pressure against position along the duct for the four duct configurations used. In each case, the appropriate static pressure at the entrance has been used as the reference. The 15 in. radius duct had a series of static tappings close to the entrance and parts (*b*) and (*c*) of figure 4 reveal that the pressure variation appropriate to the curved flow is established by about two duct widths from the entrance.

Figure 5 compares typical non-dimensional static pressure distributions across the widths of the 15 in. and 75 in. radius ducts. The continuous line shown as the calculated value was obtained from

$$p = P_1 + \frac{1}{r^2}\int_{r_1}^{r} 2r(P - P_1)\,dr,$$

where P is the total pressure, and 1 and 2 refer to the inner and outer walls, respectively, as used by Wattendorf and Eskinazi & Yeh. In the test cases, this met the outer wall static tapping pressure within the limit of accuracy expected of these readings, so that the calculation method was taken to be reliable. By comparison, it was noted that the static probe readings did show some scatter, particularly when near the walls.

Figures 6–9 show the development of the velocity distributions in the straight, 15 in. and 75 in. radius ducts. Comparison of figures 6 and 8 shows the very rapid thickening of the outer-wall boundary layer of the 15 in. radius duct, compared with that of the inner wall of the same duct and of the walls of the straight duct. The profiles of figure 8 seem to indicate that the potential-like distribution, ultimately impressed on the central region, comes from the outer wall flow. This behaviour is also revealed, although to a much lesser extent, in the profiles of figure 9, relating to the 75 in. radius duct.

Figures 10 and 12 show the variation of

$$C_f'' = 2(K_\tau/K)^2$$

with flow development and Reynolds number for the 15 in. radius duct, while figures 12 and 13 give similar information for the 75 in. radius duct and the 15 in. radius zero pressure gradient convex wall. C_f'' has been used for the local skin friction coefficient and $K_1((r_1/r_1)^2 - 1)/2\nu$ for the Reynolds number, to avoid the difficulty of the absence of a rational reference velocity.

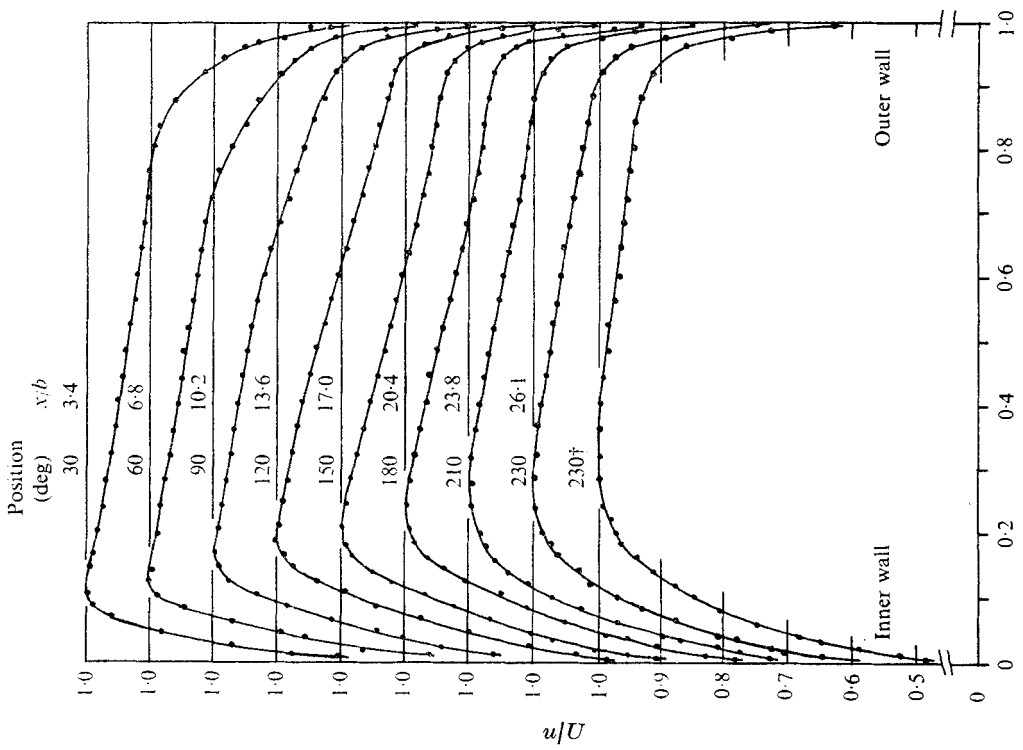

FIGURE 7. Development of velocity distribution, 15 in. radius duct.
† With boundary-layer thickeners at duct entrance.

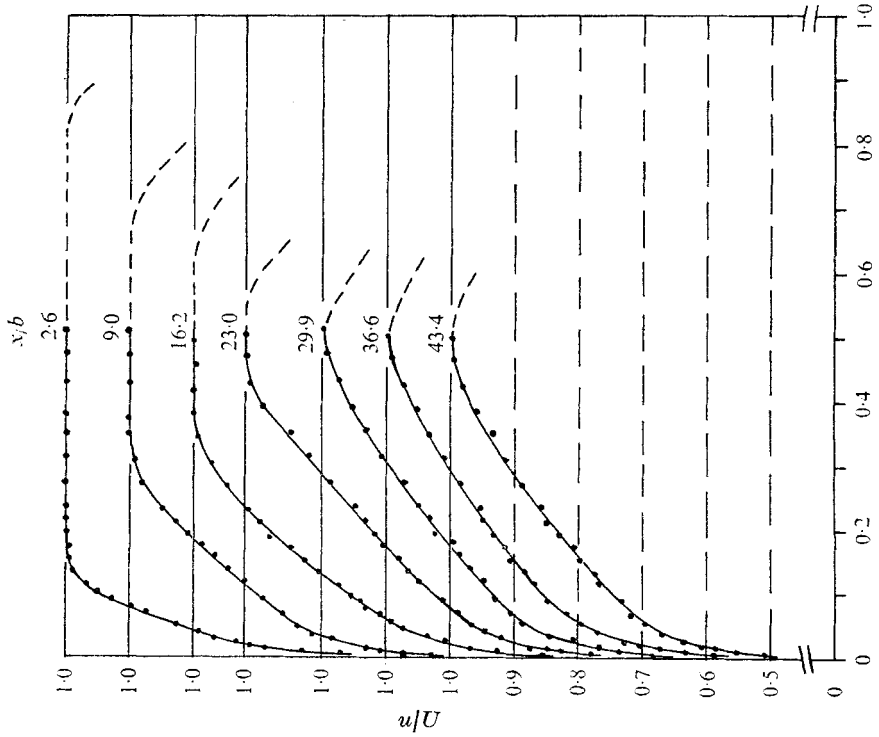

FIGURE 6. Development of velocity distribution, straight duct.

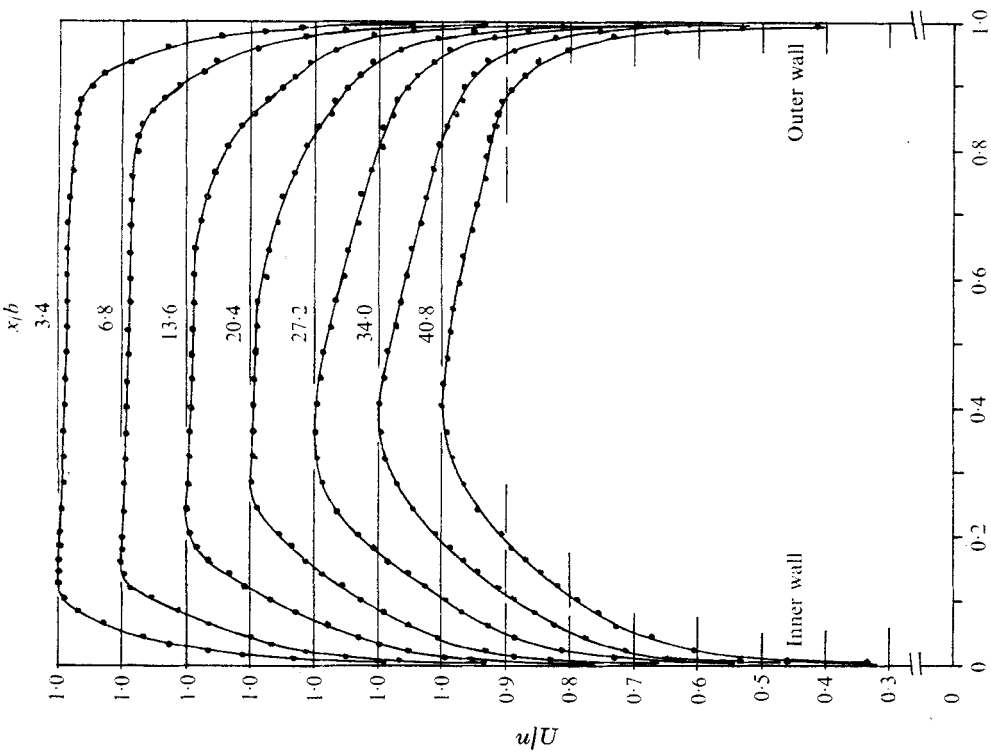

FIGURE 9. Development of velocity distribution, 75 in. radius duct.

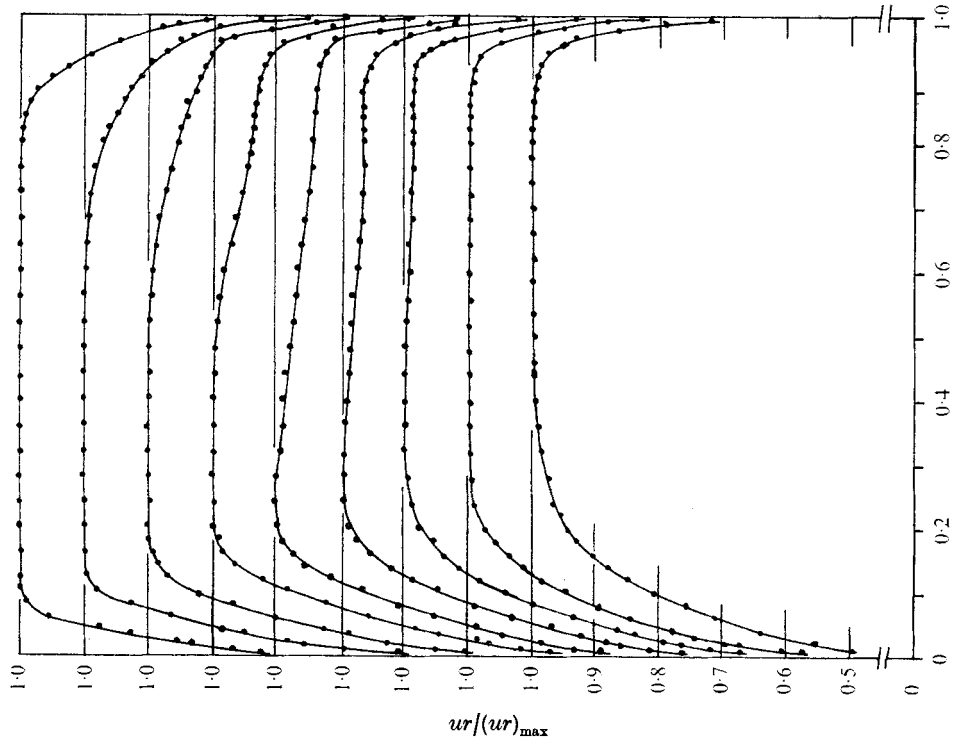

FIGURE 8. *ur* distribution, 15 in. radius duct.

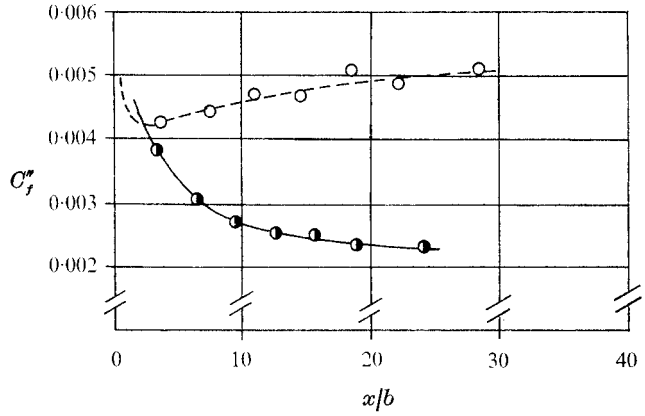

FIGURE 10. C''_f variation with flow development, 15 in. radius duct. ◑, inner; ○, outer wall.

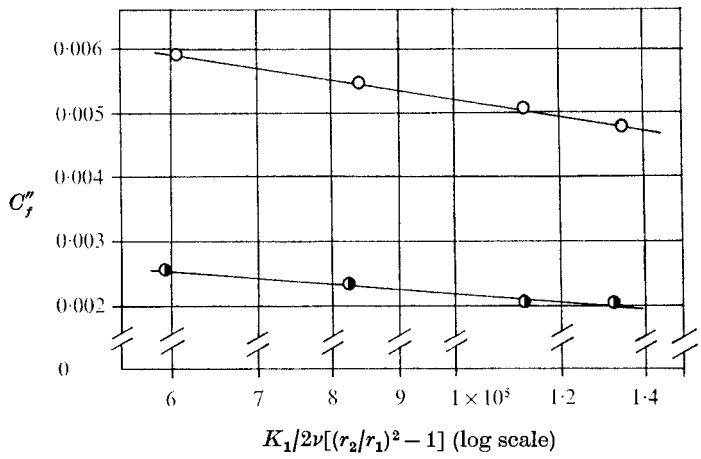

FIGURE 11. C''_f variation with Reynolds number, 15 in. radius duct. ◑, inner; ○, outer wall.

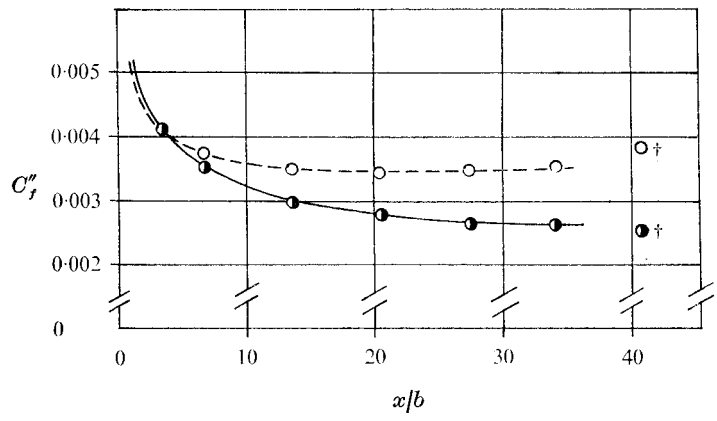

FIGURE 12. C''_f variation with flow development, 75 in. radius duct. ◑, inner; ○, outer wall.
† Points possibly affected by outlet conditions.

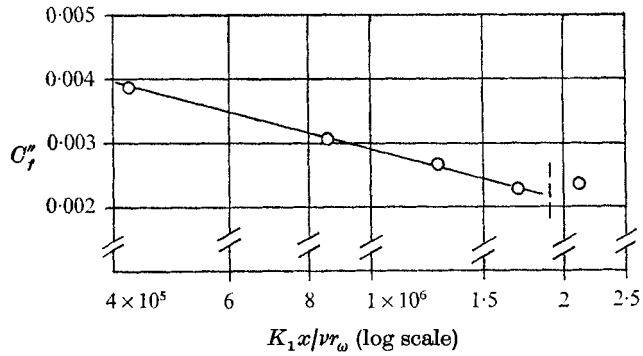

FIGURE 13. C''_f variation with distance along plate, 15 in. radius convex wall, zero longitudinal wall pressure gradient. – – –, possible onset of interference from outer wall.

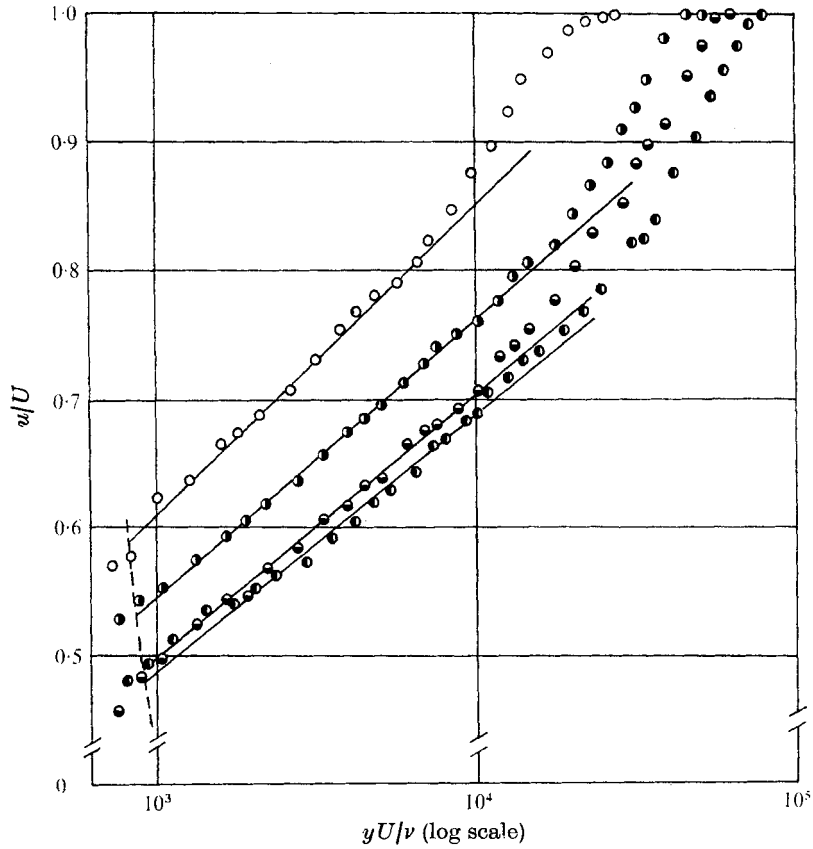

FIGURE 14. Clauser chart for developing flow, straight duct. ——, universal law.

	x/b	C'_f
○	2·6	0·00355
◑	9·0	0·00290
◒	16·2	0·00252
◐	29·9	0·00242

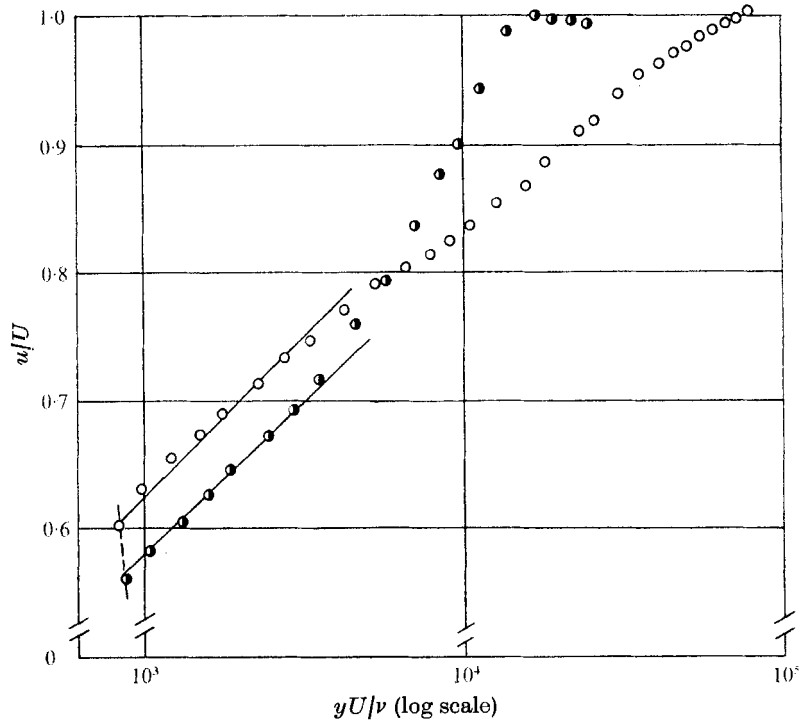

FIGURE 15. Clauser chart, 15 in. radius duct, 60° station. ◑, inner; ○, outer wall.

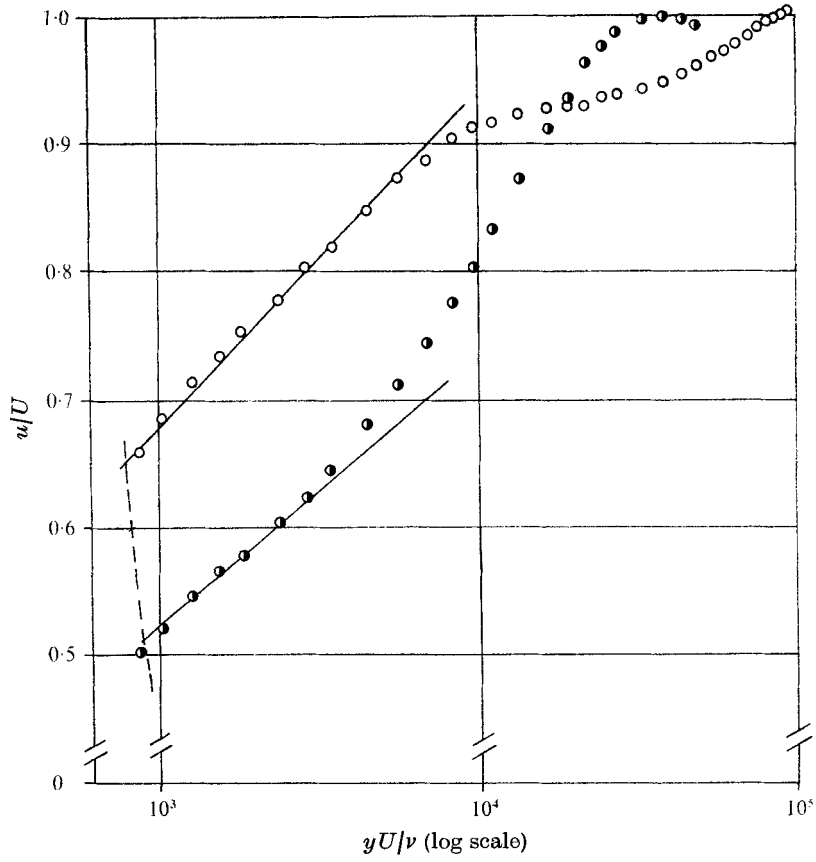

FIGURE 16. Clauser chart, 15 in. radius, 230° station. ◑, inner; ○, outer wall.

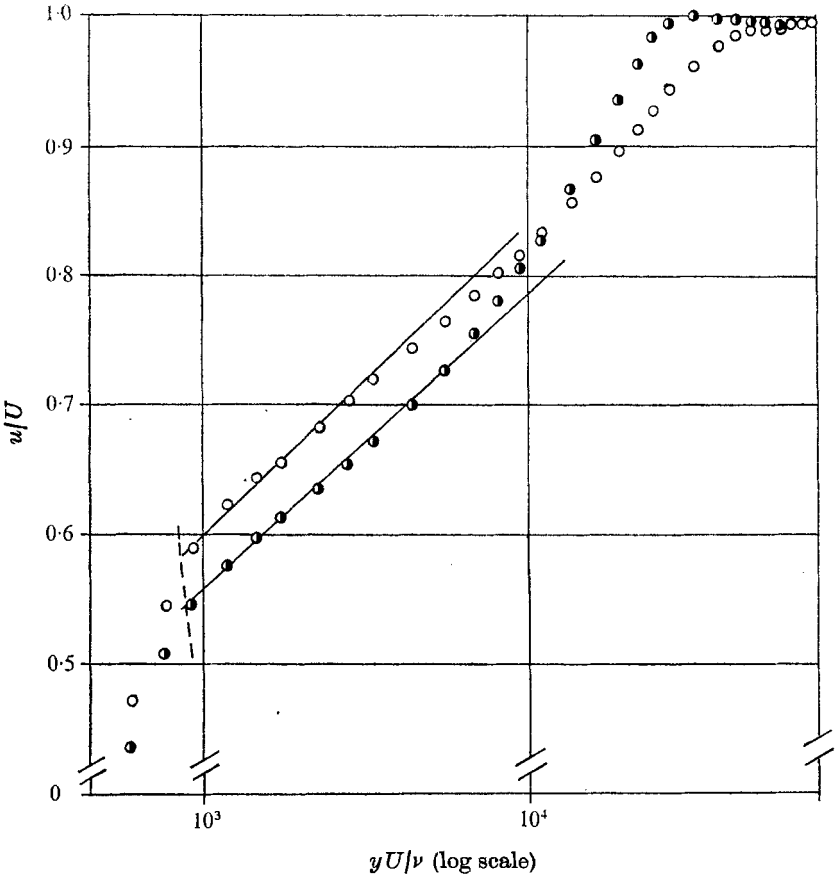

FIGURE 17. Clauser chart, 75 in. radius, station 4. ◑, inner; ○, outer wall.

4.1. *Wall region: straight duct*

As expected, the wall region of the straight-duct flows showed good correlation with the logarithmic law of the wall. Figure 14 shows a sample of four profiles plotted on a Clauser chart.

4.2. *Wall region: curved ducts*

Clauser charts were plotted for the inner and outer walls at a number of stations in both the 15 in. and 75 in. radius ducts. A sample of these plots is shown in figures 15–18. The line of best fit for $(\frac{1}{2}C_f')^{\frac{1}{2}}$ is shown on the Clauser charts. There is considerable difference between the form of these plots, and those for the straight duct in figure 14. For the inner wall, the logarithmic region is now of limited extent, even for the highly developed flows, and the outer wall plots have a characteristic droop. Inspection of figures 15–18 shows that the logarithmic law of the wall

$$\frac{u}{U_\tau} = \frac{1}{\mathscr{K}} \ln \frac{yU_\tau}{\nu} + A$$

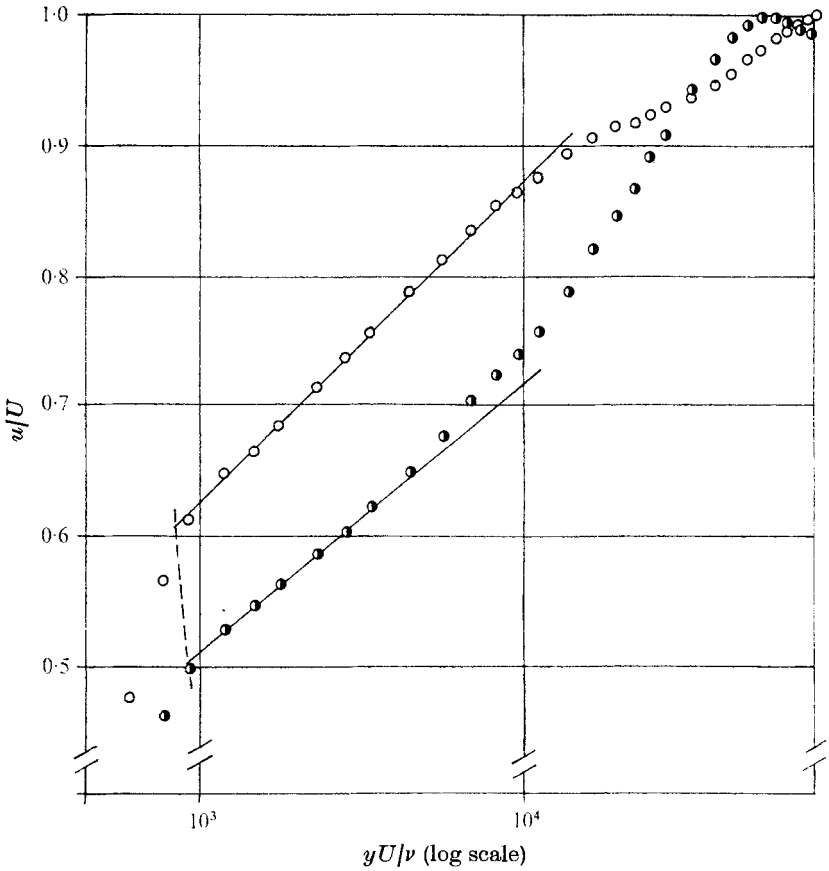

FIGURE 18. Clauser chart, 75 in. radius, station 8. ◑, inner; ○, outer wall.

can only be applicable up to quite small values of yU_τ/ν for the inner wall and is thus of limited value.

Figure 19 shows the universal plots of u/U_τ against yU_τ/ν for a random selection of twelve profiles taken from the 15 and 75 in. radius ducts. With the one exception of the curve for $r_\omega U_\tau/\nu = 96\,100$, figure 19 indicates a systematic variation with that parameter, regardless of the actual value of the curvature or other individual variables. The results thus obtained confirm that Rotta's predictions underestimate the effect of curvature, although, when comparing figure 19 with figure 1, it must be remembered that the high yU_τ/ν sections are being affected by the outer flow region. It is necessary to exercise caution in drawing any conclusions from figure 19. The U_τ values used were obtained from the C_f' values that provided the best fit for (3), and consequently at least part of the various profiles are forced to be common when plotted as u/U_τ against yU_τ/ν.

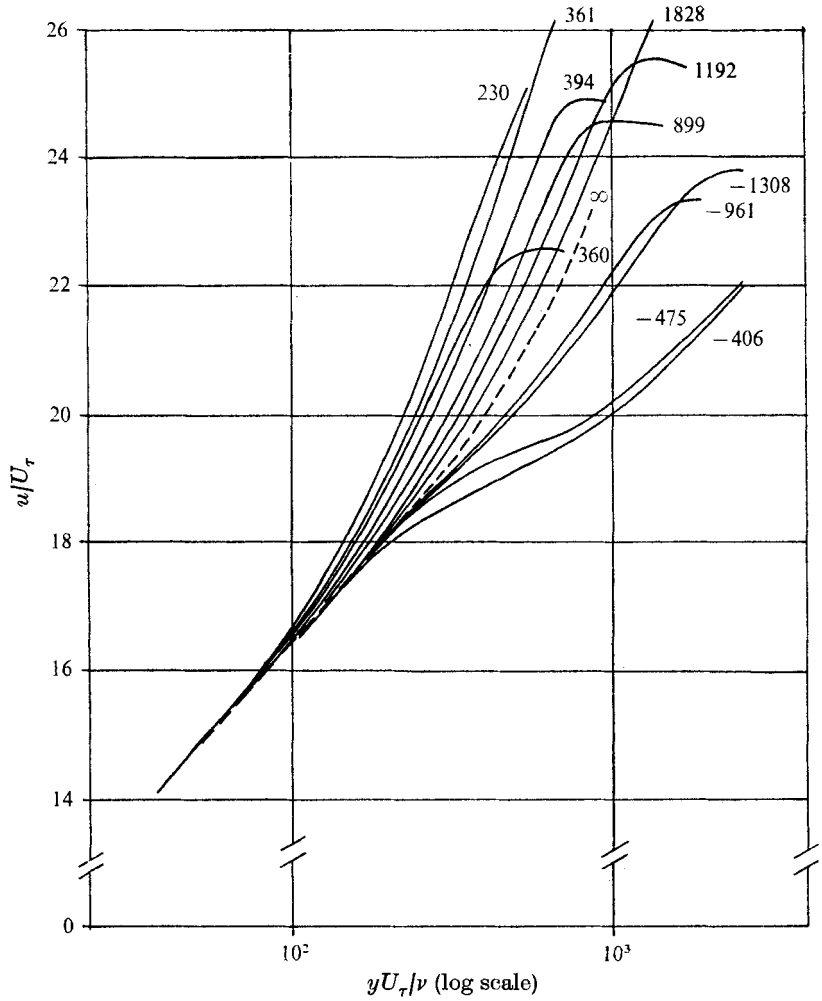

FIGURE 19. Wall region similarity, curved walls, various stations for 15 and 75 in. radius ducts. Curve labels are values of $(r_\omega U_\tau)/\nu \times 10^{-2}$.

4.3. *Core region: curved ducts*

The phenomenological approach to the determination of the mean velocity distribution requires that a knowledge be had of the shear stress distribution. In the case of fully developed curved duct flows

$$\tau = \frac{1}{2}\frac{\partial p}{\partial \phi}\left(1 - \left(\frac{r_m}{r}\right)^2\right)$$

gives such a relationship, provided r_m can be evaluated. Wattendorf made several unsuccessful attempts to evaluate r_m on theoretical grounds. The authors have had no greater success. Since the location of $r_m$is an important factor, it is worth examining the parameters that affect it. Assuming that the relevant functional relationship is

$$r_m = f(r_1, r_2, K_1, \rho, \nu),$$

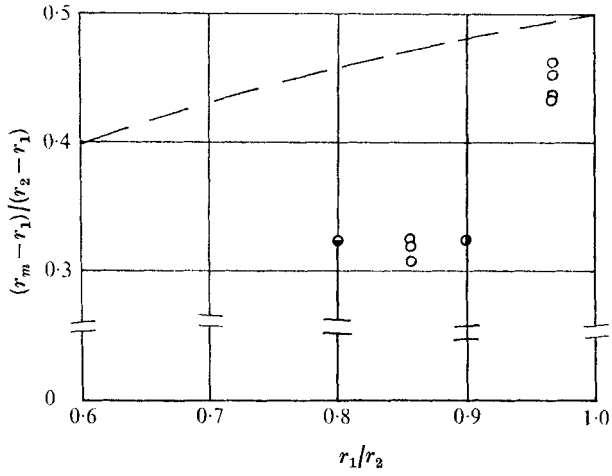

FIGURE 20. Location of zero τ as a function of r_1/r_2. – – –, laminar flow (after Eskinazi & Yeh); ◒, Wattendorf; ◑, Eskinazi & Yeh; ○, present work.

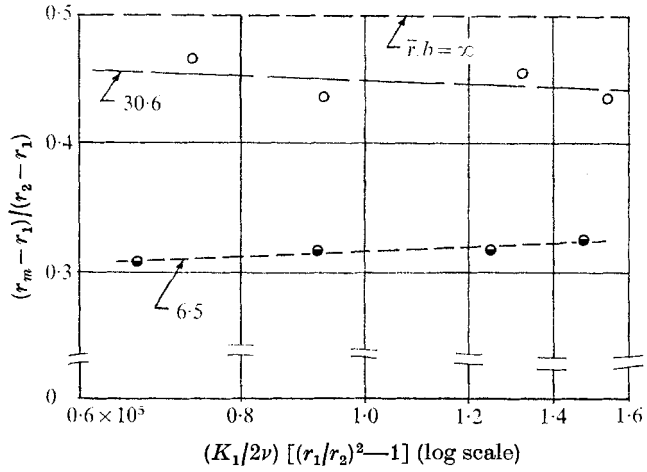

FIGURE 21. Location of zero τ as a function of Reynolds number and radius/width ratio.

dimensional analysis can be used to form three dimensionless products. Figure 20 shows the dimensionless location of the point of zero shear stress given by $\tau = 0$ at $r = r_m$ as a function of r_1/r_2. The values of r_m for the present work have been determined by the use of (6). The single values given by Wattendorf and Eskinazi & Yeh are also plotted.

Although a figure of this type was the only one given by Eskinazi & Yeh, it is apparent that the third dimensionless product, Reynolds number, could be of considerable significance. Figure 21 shows the experimental values of location of zero shear stress as a function of duct width Reynolds number and mean radius/width. Those for $\bar{r}/b = 6{\cdot}5$ (the 15 in. radius duct) show a slight consistent dependence on Reynolds number, but those for $\bar{r}/b = 30{\cdot}6$ (the 75 in. radius duct)

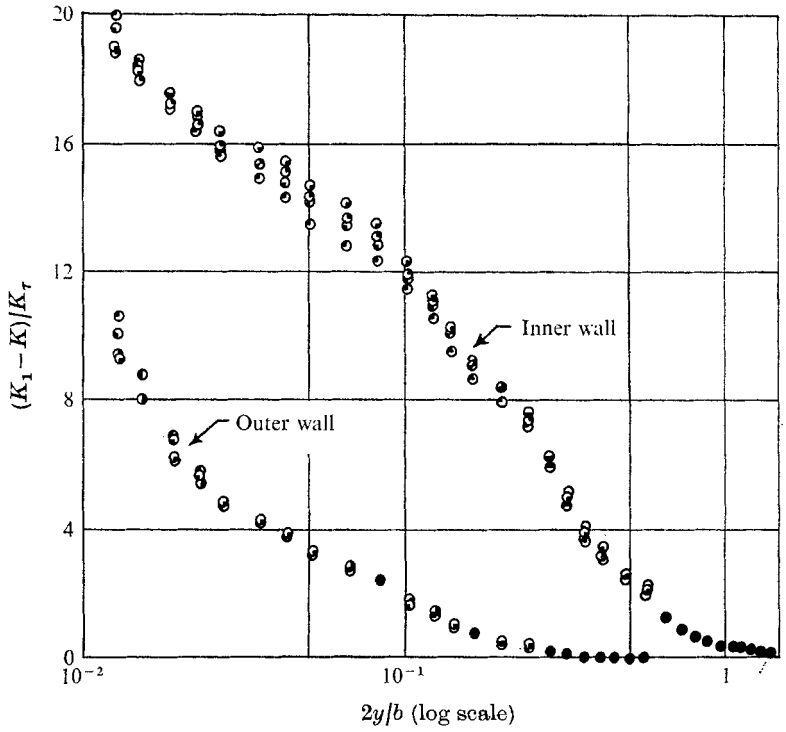

FIGURE 22. 'K' defect relationships for developed flow, 15 in. radius duct, inner and outer walls. Reynolds number ($\times 10^{-4}$): ◐, 6·1; ◐, 8·4; ◔, 11·3; ◕ 13·4.

show more scatter. It was mentioned previously that certain inconsistencies were present in the 75 in. radius duct flow, so that this scatter was not unexpected.

Wattendorf found that, although there was little difference between the non-dimensional plots of the velocity profiles for the channels of two different radii, they were each greatly different from those of the straight channel. Noting that $(r_m-r_1)/(r_2-r_1)$ must equal 0·5 for $r_1 = r_2$ (the straight duct case), figure 20 indicates that this problem is still as unresolved as it is interesting. The figure shows that the point of zero shear stress may be very sensitive to changes in mild curvature, but then becomes essentially fixed at about one third of the distance across the channel from the inner wall for curvatures above a certain amount.

Figure 22 shows the defect law

$$(K_1-K)/K_\tau = f(2y/b)$$

for a range of duct width Reynolds numbers. The results were taken at the 230° station where the flow is highly developed; both the inner and outer wall profiles are shown. The inner and outer wall profiles show a marked difference both in position and form. This would seem to indicate that Wattendorf's figure 20, has been misleadingly based on the plotting of insufficient points and that, in fact, there is no universal defect law common to both inner and outer walls. Figure 22 shows a consistent variation of the profiles with Reynolds number, particularly

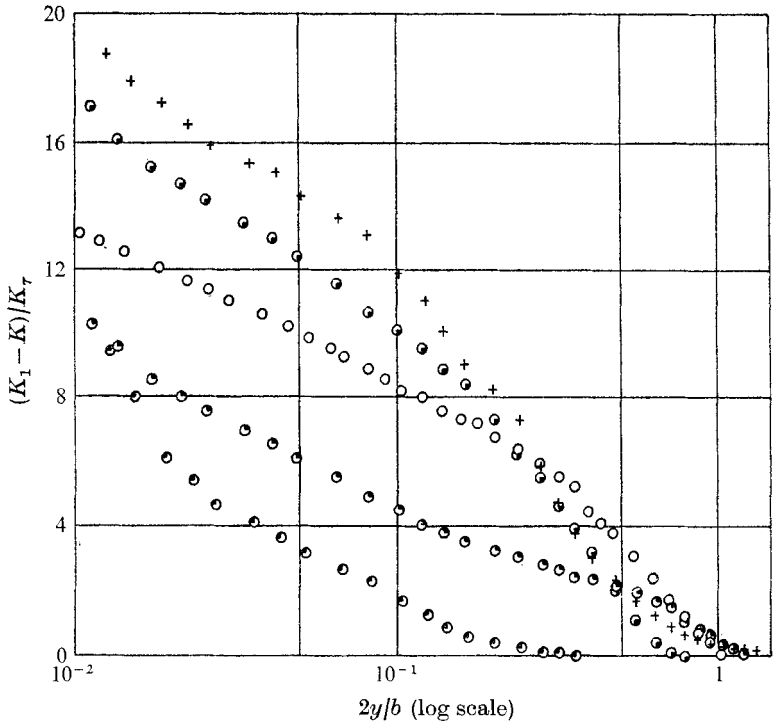

FIGURE 23. 'K' defect relationships for developed flow for various ducts at the one duct width Reynolds number. Inner: +, 15 (in. radius); ◔, 75. Straight, ○. Outer: ◐, 15; ◔, 75.

for the inner wall. Reynolds similarity would not appear to exist for the central flow region of curved ducts. In figure 23 the defect relationship has been plotted for the inner and outer sections of both the 15 in. and 75 in. radius ducts, and for the straight duct. This shows a strong dependence on radius, hence on duct radius Reynolds number.

The application of (5) which followed from the extension of Kinney's analysis to the fully developed flow situation was unsuccessful, it being found impossible to obtain a value of K_4 which provided a good fit to any one profile.

4.4. *Outer region of convex wall boundary layer*

The findings of § 4.3 indicate that it is unlikely that a universal defect law exists for the outer region of a curved wall boundary layer, even for the simplified case of zero longitudinal wall pressure gradient. Figure 24 shows that this is the case.

5. Conclusions

(i) The behaviour of a curved shear flow has been found to be unlike that of a plane shear flow. The rate of growth of the boundary layers and the values of the skin friction coefficients obtained indicate that the turbulence tends to be suppressed on the convex wall and amplified on the concave wall, and this is in agreement with the classical Rayleigh stability criteria.

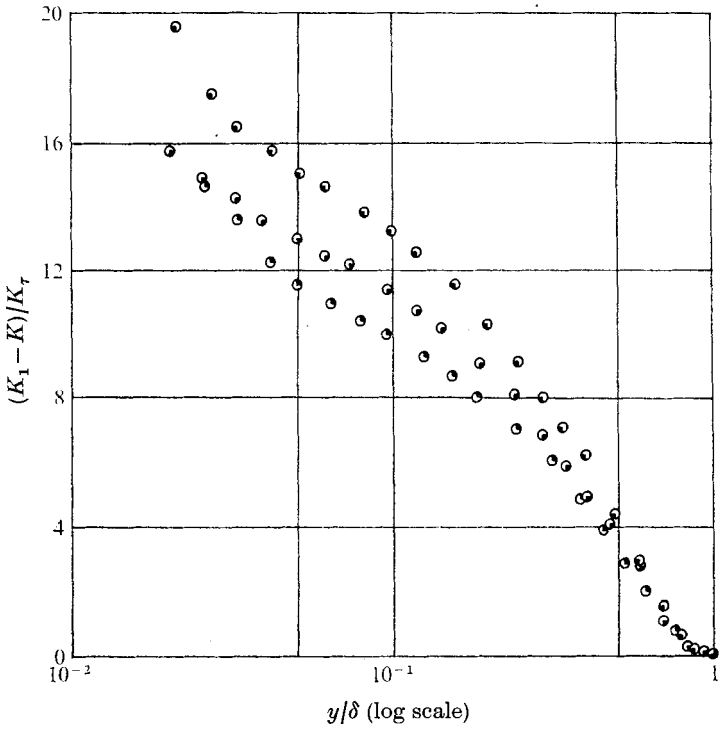

FIGURE 24. 'K' defect relationships for developing flow, 15 in. radius convex wall, zero longitudinal wall pressure gradient.

Station (deg)	$(K_1 x)/\nu r_\omega$ ($\times 10^{-5}$)
60	8·7
90	12·9
120	17·2

(ii) Similarity of the mean flow, as represented by a defect type law, does not exist on the basis of mean velocity, ur or u/r for either fully developed curved channel flow or the outer regions of convex wall boundary layers.

REFERENCES

BRADSHAW, P. 1965 *J. Fluid Mech.* **22**, 679.

CLAUSER, F. 1954 *J. Aero. Sc.* **21**, 91.

ELLIS, L. B. 1969 M. Engng Sci. thesis, University of Melbourne.

ESKINAZI, S. & YEH, H. 1956 *J. Aero. Sci.* **23**, 23.

GÖRTLER, H. Z. 1941 *Z. angew. Math. Mech.* **21**, 250.

KAYE, J. & ELGAR, E. C. 1958 *Trans. A.S.M.E.* **80**, 753.

KINNEY, R. B. 1967 *Trans. A.S.M.E.* E **34**, 437.

MACMILLAN, F. A. 1957 *Aero. Res. Counc. R. & M.* no. 3028.

MARRIS, A. W. 1956 *Can. J. Phys.* **34**, 1134.

MARRIS, A. W. 1960 *Trans. A.S.M.E.* D **82**, 528.

MURPHY, J. S. 1962 *J. Aero. Sci.* **29**, 366.

ROTTA, J. C. 1962 *Progress in Aeronautical Sciences* (ed. A. Ferri, O. Küchemann and L. H. G. Sterne), vol. 2, p. 1. Pergamon.

ROTTA, J. C. 1967 *Phys. Fluids Suppl.* **10**, 5174.

SCHULTZ-GRUNOW, F. & BREUER, W. 1965 *Basic Developments in Fluid Dynamics* (ed. M. Holt), vol. 1, p. 377. Academic.

TANI, I. 1962 *J. Geophys. Res.* **67**, 3075.

TAYLOR, G. I. 1922 *Phil. Trans.* A **223**, 289.

TAYLOR, G. I. 1932 *Proc. Roy. Soc.* A **135**, 685.

THOMANN, H. 1968 *J. Fluid Mech.* **33**, 283.

TILLMANN, W. 1967 *Phys. Fluids Suppl.* **10**, S108.

TOWNSEND, A. A. 1956 *The Structure of Turbulent Shear Flow*. Cambridge University Press.

TRAUGOTT, S. C. 1958 *N.A.C.A. Tech. Note*, no. 4135.

YEN, K. T. & TOBA, K. 1961 *J. Aero. Sci.* **28**, 877.

WATTENDORF, F. L. 1935 *Proc. Roy. Soc.* A **148**, 565.